Spring 2014

Re-analysis of the World Data on the EMC Effect and Extrapolation to Nuclear Matter

Stacy E. Karthas
University of New Hampshire - Main Campus, seo734@wildcats.unh.edu

Re-analysis of the World Data on the EMC Effect and Extrapolation to Nuclear Matter

Stacy E. Karthas

May 15, 2014

Abstract

The EMC effect has been investigated by physicists over the past 30 years since it was discovered at CERN. This effect shows that the internal nucleon structure varies when in the nuclear medium. Data from SLAC E139 and JLab E03 103 were studied with the Coulomb correction and directly compared. The Coulomb distortion had a greater impact on the JLab data due to slightly lower energies and different kinematics. The EMC ratio was found to have a dependence on a kinematic variable, ϵ, which was removed when Coulomb corrections were applied. The methodology was developed to apply Coulomb corrections, which had been neglected in the past, and to extrapolate to nuclear matter to compare to theory. From the result of the analysis presented in this document, different experiments may be combined to produce one data set.

Contents

1 Introduction

Often, experiments are used to test theoretical models and ideas. In the process of testing these ideas, it is more interesting when something unexpected is discovered. Modern science teaches that these moments lead to a better understanding of the world because of the questions sparked through their discovery. A 30 year old anomaly has continued to puzzle nuclear physicists in the form of the European Muon Collaboration (EMC) Effect. This effect indicates a difference in the substructure of nucleons when they are contained in a heavy nucleus and to those in a free nucleons.

However, though this effect has been known to physicists for more than 30 years, it is still not fully explainable by theory. When comparing theory to experiment, it is necessary that experimental results are as accurate as possible with corrections made where applicable. The goal of this project was to add a non-negligible correction to the current world data and to examine whether or not it is possible to compare the data from two different experiments. This added correction will improve the accuracy of the two data sets by accounting for an important factor that affects the results.

1.1 The EMC Effect

The EMC Effect was first discovered in 1983 by the European Muon Collaboration while comparing their muon scattering data for a heavy nuclei target, iron, to that of a light nuclei target, deuterium. The collaboration was planning to probe the substructure of free nucleons. Therefore, their experiments were performed in the deep inelastic scattering region where the leptons probe the quarks within the struck nucleon. The drastic difference in mass of the two targets resulted in an unexpected find. The collaboration hoped to use a heavy nuclei target to extract the free nucleon structure function. It was understood that it would be necessary to understand how the heavy nucleus would affect the experimental result since the nuclear density is much higher. This higher density was desired to take more data. It was known that the heavier targets would differ from the lighter targets because of the higher binding energy in the nuclei. However, the binding energy is much smaller than the beam energy and so it should be negligible. Before the EMC effect was discovered, and during the initial attempts to describe the anomaly, it was only known how to correct for nucleon motion. Aubert's original paper [1] in 1983 was the first to discuss that the corrections for nucleon motion did not account for all the differences in structure functions between heavy nuclei nucleons and the free nucleons.

The EMC ratio used in this report is:

$$R_{EMC} = \frac{\sigma_A}{\sigma_D}\frac{2}{A}, \tag{1}$$

where σ_A is the lepton cross section of a nucleus with mass number A, σ_D is the lepton cross section of deuteron. In the original paper, and in many subsequent studies, the structure function F_2, as will be discussed in Section 1.2, was used in the ratio instead of the cross section. The ratio $\frac{2}{A}$ is to correct for the number of nucleons in each nucleus so as to compare the cross sections of one nucleon from each nucleus.

The ratio of cross sections in a specific deep inelastic scattering region with respect to x, ratio of momentum of the struck quark, were expected to be about one for most $x < 0.8$. However, the collaboration discovered this was not the case. The ratio, Equation 1, had an unexpected dip below one, as demonstrated in Figure 1, that could not be accounted

for by models available at the time. This would suggest that the quark momentum distributions would differ for nucleons in heavy and light nuclei. This is further discussed in Section 1.2.

The EMC effect is still not completely explainable by theory. Therefore, it is necessary to ensure the experimental analysis is as complete and accurate as possible. All non-negligible corrections must be made as well as analyzing the data so that it may be compared to theory. The data can, currently, only be compared to theory in the case of light nuclei and infinitely heavy nuclei, nuclear matter.

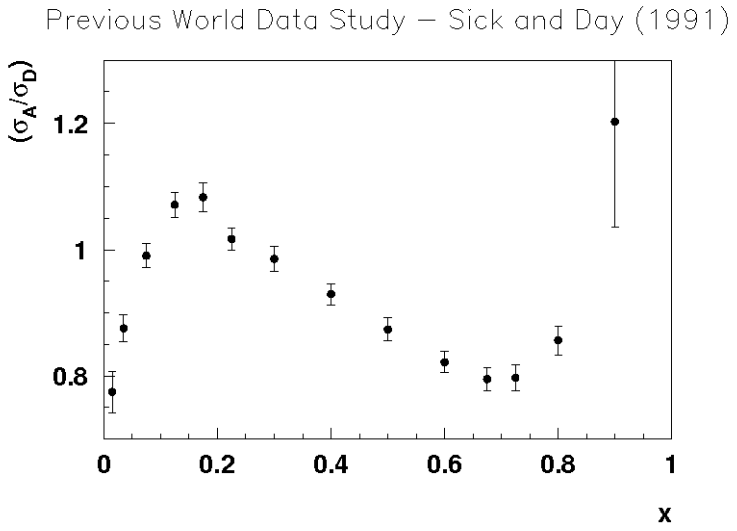

Figure 1: The previous analysis, performed by Sick and Day, with extrapolation to nuclear matter. [2]

I. Sick and D. Day, performed an analysis of the EMC effect [2] on nuclear matter for multiple experiments and published their results, as illustrated in Figure 1. The correction for the distortion of the cross section due to the Coulomb force, acting on the incoming and outgoing charged leptons,was not considered by Sick and Day, but it makes a non-negligible difference in the EMC ratio. As well, if this Coulomb correction is not applied, the comparison of multiple data sets directly may not be valid. This report makes improvements to their method by adding this correction and analyzing data from an experiment at the Thomas Jefferson National Laboratory Facility (JLab) in conjunction with an experiment at SLAC National Accelerator Laboratory (SLAC).

1.2 Deep Inelastic Scattering

In scattering experiments, the lepton particle beam will scatter from a target nuclei. Scattering experiments are used to probe the structures of target nuclei and atoms. This scattering is initiated through the exchange of a photon. It is this high energy photon exchange that causes the electron to scatter at an angle from the nucleus. The scatter is described by Quantum Electrodynamic interactions since the leptons are point-like particles and have no structure of their own. Therefore, through scattering, leptons can be used to gather information about the target nucleus. The scattering cross section is measured experimentally. This scattering cross section is dependent upon structure

functions which define aspects of the internal structure of the nucleons including charge and momentum distributions of quarks. Thus, from the scattering cross section of the lepton, one can extract the internal structure of the target.

This project is concerned with an effect visible in the deep inelastic scattering region (DIS). At the increased energy levels, the beam of probing particles, electrons, positrons, or muons, are able to penetrate to the quark level. Henceforth, the probing particles will be referred to as electrons as both experiments analyzed in this project used electron beams. The momentum transferred to the struck nucleon is large enough at these energy levels to cause the momentum to be transferred directly to individual quarks. This region allows physicists to investigate the substructure of the nucleons within the nucleus. Figure 2 illustrates an incident electron scattering from an individual quark. When analyzing DIS experiments, there are specific variables that are important to consider and will be outlined below [3].

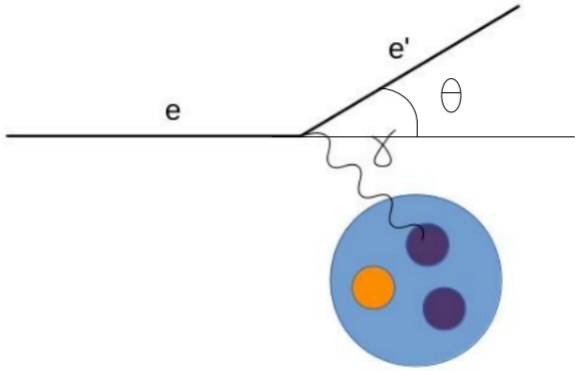

Figure 2: The deep inelastic scattering region probes the internal structure of the nucleon by exchange of a virtual photon between the lepton and the struck quark. The Lepton scatters at an angle θ as shown in the figure.

As discussed previously, the EMC effect is primarily concerned with the substructure of nucleons within heavy and light nuclei. Figure 2 illustrates a struck quark of a free nucleon while Figure 3 illustrates a possible quark distribution for nucleons within a heavy nuclei. One possible explanation for the EMC effect is the quarks in nucleons of heavy nuclei having more space to occupy. This may be due to a sharing of quarks between multiple nucleons as diagrammed in Figure 3. Close contact nucleons may share some spatial extent, and thus, their quarks may be able to freely move in some region of the neighboring nucleon. The nucleons seem to be deformed slightly in this process as well.

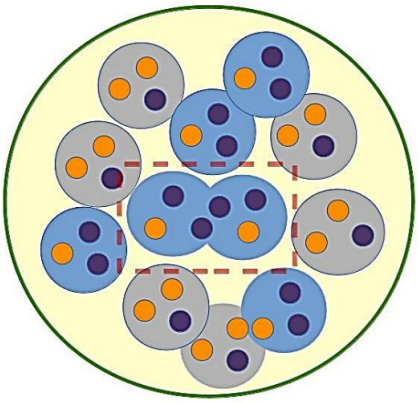

Figure 3: A possible explanation for the EMC effect is the nucleons in a heavy nucleus sharing quarks. The substructure of nucleons within a heavy nucleus is different than free nucleons as in Figure 2.

Assuming an incident energy of E and scattered energy of E', the transferred energy to the nucleon by the incident electron is E-E', referred to as ν. This is used to describe the kinematics of the experiment and so is an important part of the cross section formula. Other important quantities used to describe the kinematics are the invariant mass in Equation 2, the four-momentum transfer in Equation 3, and the Björken variable x as in Equation 4.

$$W^2 = M^2 + 2M\nu - Q^2, \tag{2}$$

where M is the mass of the proton.

$$Q^2 = 4EE'sin^2\frac{\theta}{2}, \tag{3}$$

where θ is the scattering angle as in Figure 2.

$$x = \frac{Q^2}{2M\nu} \tag{4}$$

This variable, x, is used to combine the important four-momentum transfer, Q^2 with the energy transferred to the struck quark. This quantity will be used throughout this study since it is used to define the DIS region and encompasses multiple features of the kinematics. In addition to these variables, another variable that will be used in the analysis is the value ϵ as in Equation 5 and will be more thoroughly described in Section 5.

$$\epsilon = \frac{1}{1 + 2(1 + \nu^2/Q^2)tan^2\frac{\theta}{2}} \tag{5}$$

These variables are brought together in the cross section formula.

$$\sigma = \frac{d^2\sigma}{d\Omega dE'} = \frac{\alpha^2 cos^2\frac{\theta}{2}}{4E^2 sin^4\frac{\theta}{2}}\left(\frac{2}{M}F_1(x,Q^2)tan^2\frac{\theta}{2} + \frac{1}{\nu}F_2(x,Q^2)\right) \tag{6}$$

Where $F_{1,2}$ are the structure functions and α is the fine structure constant.

The cross section formula, as detailed in Equation 6, accounts only for single hard photon exchange and thus, neglects multi-photon exchanges. Because the scattering cross section is dependent on form factors which are used to describe the internal structure of the target, it is a necessary quantity for scattering experiments. The structure functions can be determined through models for the theoretical predictions used to find the Coulomb corrections as will be described in Section 2.1.1. The scattering cross section can be determined experimentally and is therefore analyzed to study the structure of the nucleus.

1.3 Experiments Analyzed

Since the EMC effect was first discovered in 1983, there have been many studies to repeat the experiment, or similar, to reproduce the data. The experiment has been performed at many energies and for many targets. The two experiments analyzed in this thesis project were SLAC E139 and JLABE03 103 since these are the most complete and precise sets of data. The following sections provide a brief overview of the experiments.

1.3.1 SLAC E139

The SLAC E139 experiment was performed at the SLAC Linear Accelerator Facility which provided an electron beam of energy in the range of 8.0 to 24.5 GeV. The electrons were scattered from targets of ^{4}He, ^{9}Be, ^{12}C, ^{27}Al, ^{40}Ca, ^{56}Fe, ^{108}Ag, and ^{197}Au. Deuterium is also used to produce the EMC ratio. The detector used in this experiment was a magnetic spectrometer which included a C̃erenkov detector and electromagnetic calorimeter. The cross sections were gathered from these detectors for each of the targets.

Previous analysis had been performed for this experiment by Gomez, et al. as in [4] and some data from this experiment had been used by Sick and Day in [2]. However, more extensive analysis of data from this experiment is important for comparison to theory and other experiments.

1.3.2 JLabE03 103

The JLabE03 103 experiment was performed at JLab using the Continuous Electron Beam Accelerator Facility (CEBAF) electron beam providing electrons to Hall C. CEBAF produced electrons with a beam energy of 5.766 GeV. The electrons were scattered from solid and cryogenic targets of ^{3}He, ^{4}He, ^{9}Be, ^{12}C, ^{63}Cu, and ^{197}Au. As in SLAC E139, Deuterium is also used to produce the EMC ratio. The electrons were then focused through and into detectors of the High Momentum Spectrometer. The scattered electrons are tracked in the drift chamber, through a C̃erenkov detector, and ultimately detected in the calorimeter, used for particle identification. By counting these particles, it is possible to extract the cross sections and therefore the EMC ratio.

An extensive analysis has already been performed for the JLabE03 103 experiment for light nuclei [5], but not yet for the heavy nuclei completely. Thus, the analysis of the heavy nuclei target data from this experiment was the focus of this report.

2 Re-Analysis of World Data

Since the EMC ratio is measured from experiments at different kinematics, it is necessary to develop a methodology to compare the two data sets. In this experiment, it was necessary to correct for inconsistently applied corrections including Coulomb corrections. Theoretical models are available for nuclear matter. So, after the corrections were made, the results may be compared to theory.

2.1 Corrections

The following corrections were inconsistently applied. In this thesis project, I have performed these corrections on world data to produce more accurate data that will be comparable to current theoretical models. Coulomb corrections must be applied in the energy ranges and with the targets used in the JLab and SLAC experiments.

2.1.1 Coulomb Correction

In DIS experiments, like the experiments used for this analysis, the particles that approach the target are affected by the Coulomb field produced by the target nuclei. This results in a distortion of the path of the incident and scattered particles. Assuming an electron beam, the particles accelerate in incidence and decelerate in scattering due to electromagnetic interactions. The correction has been incorrectly applied in previous analyses since it has been neglected at certain energies. However, it has been shown by Solvignon, et al. in [6] and will be reaffirmed in this paper that the energies used at JLAB and SLAC do not result in negligible Coulomb corrections.

In scattering interactions, a virtual photon is exchanged as the primary interaction between the electron and the struck quark. This virtual photon is highly energetic and is called a hard photon. The electromagnetic force carrying particle is the photon. Therefore, as the electron passes through the positively charged target, soft, i.e. less energetic, photons are exchanged as illustrated in Figure 4. This extends the standard one photon exchange model to a one hard photon and several soft photon exchanges [7].

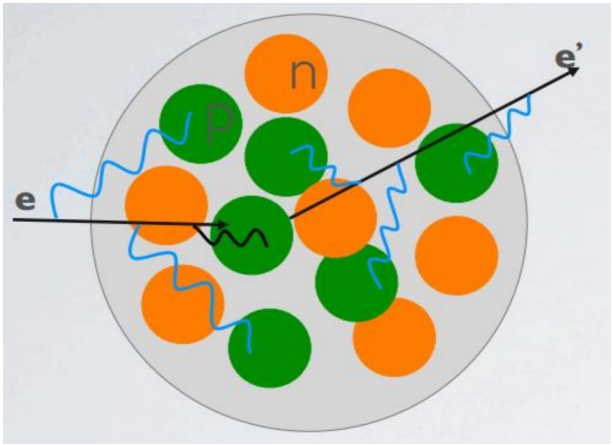

Figure 4: As the electron beam scatters from a heavy nucleus, it interacts with the quark of a nucleon through the exchange of a hard photon (black) and is accelerated and decelerated by the Coulomb interactions through the exchange of soft photons (blue).

The electrostatic potential inside the nucleus can be approximated as that of the potential inside of a charged sphere [6].

$$V(r) = \frac{-3\alpha(Z-1)}{2R} + \frac{\alpha(Z-1)}{2R}\left(\frac{r}{R}\right)\hbar c, \tag{7}$$

where Z is the number of protons in the nucleus, r is the distance from the center of the charged sphere, and R is the radius of the sphere defined by :

$$R = 1.1A^{1/3} + 0.86A^{-1/3}, \tag{8}$$

where A is the atomic mass number of the nucleus. In a nucleus, the effective Coulomb potential can be approximated to be $\overline{V} = 0.75V(0)$ as has been shown in [8]. In their study, they came to the conclusion that Coulomb distortions can be corrected for using this potential. The additional potential must be added to the incident and scattered electron energies when calculating the cross section since the Coulomb potential will be significant in comparison to the beam energy for heavy nuclei. The effective potential can be as much as 19 MeV for the targets used in the experiments analyzed in this report. When the incident beam energies are on the order of 12 GeV or less, and so the scattered beam energy is even smaller, the effective potential is a non-negligible fraction of the beam energy. Therefore, it is important at such energies to account for this distortion.

The Coulomb distortion is not as necessary to perform for light nuclear targets because the electrostatic potential will be significantly smaller since it is dependent heavily on Z. As the number of protons that form the nucleus, the positive charge of the nucleus will increase. Therefore, the electrostatic force and potential will both increase. The Coulomb corrections for the two lightest nuclei in this study, deuterium and helium-4, are so similar they do not need to be applied in this case. Since the cross sections for all nuclei in this study are compared with that of deuterium, the Coulomb correction is only required for nuclei very different from deuterium.

When Coulomb corrections are applied to the cross section, the incident and scattering energies are replaced by a Coulomb corrected initial and final energy denoted as $\overline{E} = E+\overline{V}$ and $\overline{E'} = E' + \overline{V}$, respectively. A new Q^2, W^2, and x value must be calculated as well since each is dependent upon these new effective incident and scattered energies. A model for the form factors, $F_{1,2}$, necessary to calculate the cross section is available [9]. This model used was based on empirical fits and is valid in the kinematics region studied in this paper. This model requires the value of A, Z, Q^2, and W^2. Therefore, the cross section model can be used to find a Coulomb corrected cross section and a non-corrected cross section. Since the deuterium cross section is not affected by the Coulomb distortion, only the heavy nuclei Coulomb corrections must be calculated. Equation 9 was used to calculate each Coulomb correction factor:

$$CC = \frac{\sigma_{CC}}{\sigma} * F^2, \tag{9}$$

with

$$F = \frac{E + \overline{V}}{E}. \tag{10}$$

σ_{CC} is the Coulomb corrected model cross section, σ is the original model cross section, and F is the focusing factor. The focusing factor accounts for the nucleus acting like a lens to focus the wave function of the electron [10]. The form factors found from the

model were used as in Equation 6. The incident energy in the cross section equation was adjusted for the Coulomb distortion by adding the effective energy.

Figures 5 and 6 illustrate how this Coulomb correction factor is dependent on the atomic mass number of the nucleus. As discussed earlier, the Coulomb correction factor will increase with the atomic mass number since the Coulomb potential is more significant.

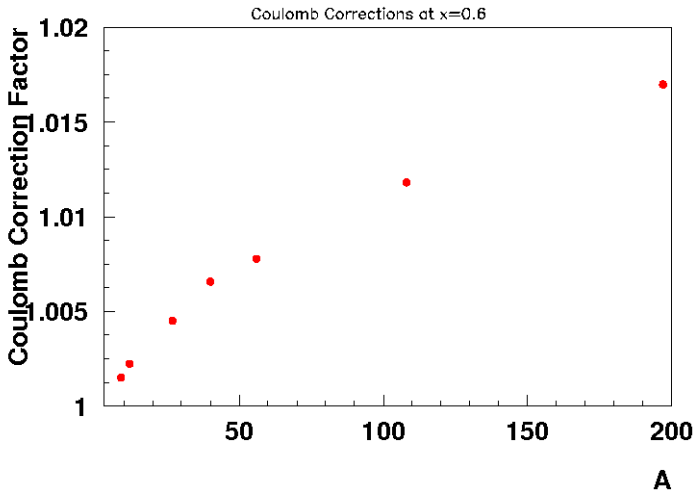

Figure 5: Dependence of the Coulomb correction factor on the atomic mass number A. These Coulomb corrections are for the SLAC E139 kinematics at x=0.6.

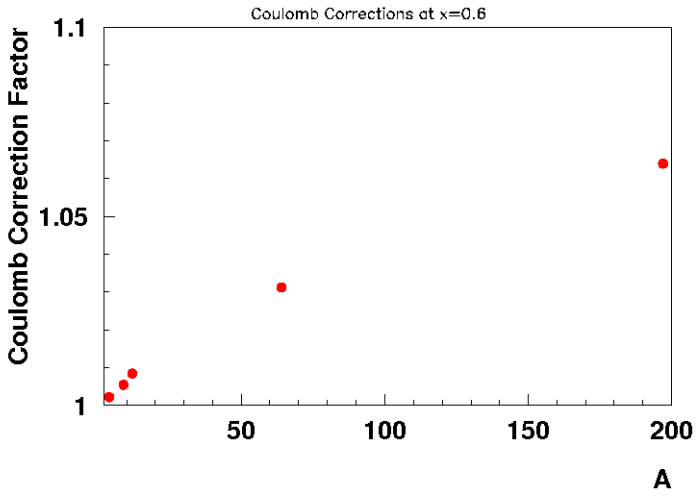

Figure 6: These Coulomb corrections are for the JLabE03 103 kinematics at x=0.6.

The two experiments analyzed in this paper were run at different energies, so each of the Coulomb corrections had to be applied separately for each target at both experimental kinematics. The Coulomb corrections are significant when the beam energy is small. This is because the Coulomb potential will be a reasonable percentage of the beam and scattered energies and so will make a large adjustment to the cross section. Similarly, if the nucleus is heavy enough, the Coulomb potential will be large enough to make an

impact on the cross section since it will make a significant change to the effective energy of the beam. This effect is demonstrated when comparing Figures 5 and 6. The beam energy for the JLab and SLAC experiments respectively were 5.766 GeV and 8.0-24.5 GeV. Therefore, the Coulomb correction factors for the smaller energy experiment, JLab, were significantly increased.

The reason the Coulomb distortion is especially important to the EMC ratio is because it results in an overestimate of the EMC effect. As is evident in Figure 7, the EMC ratio is increased significantly by the addition of Coulomb corrections to the analysis. In the heaviest target analyzed,the Coulomb corrections increase the EMC ratio at most two percent for the SLAC experiment and as much as 10 percent for the kinematics region analyzed for the JLAB experiment. This difference is mostly because the beam energy for JLAB is smaller than that of SLAC.

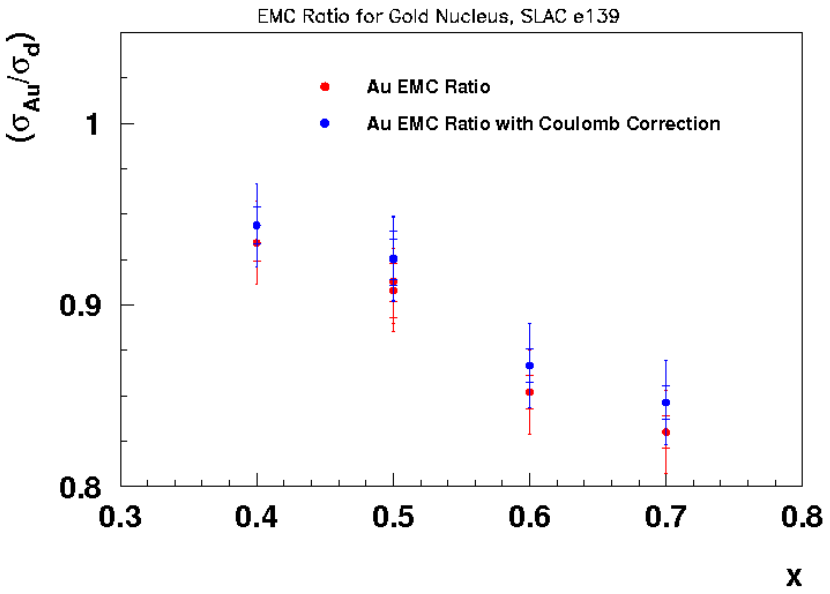

Figure 7: EMC ratio for gold target with and without Coulomb corrections applied for kinematics and data from SLAC E139.

3 Extrapolation to Nuclear Matter

Since the EMC effect was an anomaly, many theories had to be proposed to predict why the effect occurred. Thus, models are produced in order to test theories against the data experiments have measured.

Nuclear structure can be solved through the Schrödinger equation for light nuclei and for infinitely heavy nuclei. The experimental data has been analyzed with theory for the former in [5] and [11] comparing to few-body theory. Figure 1 shows the previous analysis for extrapolation to nuclear matter performed by Sick and Day in [2]. This is a study of the latter, infinitely heavy nuclei. However, this analysis included SLAC data as well as neglecting the Coulomb corrections considered.

Infinitely heavy nuclei are those with an infinite number of nucleons in the nucleus.

This is known as nuclear matter and will be the topic of the rest of this paper. Since there are no experimental nuclear matter targets, it is necessary to use the available target nuclei data and extrapolate to nuclear matter through a linear analysis as in [2].

3.1 EMC Ratio Dependence on $A^{-1/3}$

As described in [12], the cross section has a contribution proportional to the radius of the nucleus squared, $R^2 = (r_0 * A^{1/3})^2$. Thus, when the EMC ratio is considered as in Equation 1, the EMC ratio is proportional to $\frac{A^{2/3}}{A} = A^{-1/3}$. A comparison between this quantity and the EMC ratio can be used to extrapolate to nuclear matter.

Data for each kinematic x must be plotted separately since the EMC ratio is dependent upon x. Also, in the extrapolation, each experiment must be analyzed separately because of the different experimental kinematics, that is values of Q^2, E, E', and ν. Figure 8 depicts the extrapolation to nuclear matter for x=0.5 for SLAC E139. Since nuclear matter will have infinitely many nucleons, we are able to extrapolate to the y-axis, that is $A^{-1/3} = 0$. A linear fitting routine is used to find the slope and y-intercept along with their associated errors due to the fit and the errors attributed to each of the data points.

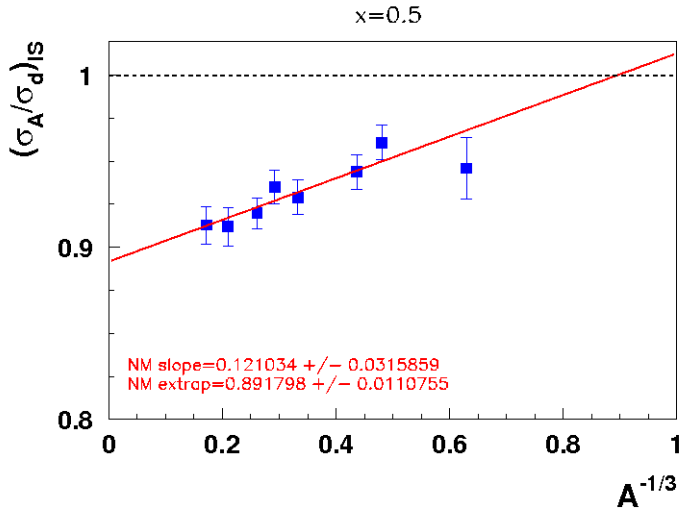

Figure 8: The EMC ratio for nuclear matter extrapolated to the y intercept from SLAC E139 with $Q^2 = 5$ and x = 0.5, when the EMC ratio is plotted against $A^{-1/3}$.

Once this extrapolation is performed for each x (x = 0.4, 0.5, 0.6, and 0.7), the nuclear matter EMC ratio is plotted against these x values to produce an EMC effect curve. An example of this curve for SLAC E139 is located in Appendix C. This curve illustrates the differences between extrapolations using the dependence on $A^{-1/3}$ and dependence on density.

3.2 EMC Ratio Dependence on Density

The maximum nuclear density is 0.17 nucleons per fm^3 and it is used as the density of nuclear matter. The same analysis can be performed using the nuclear density as was performed using the A-dependence to extrapolate to nuclear matter. In this analysis, we

used two different density calculations. The first is the density assuming the nucleus is a uniform sphere. The second uses a more detailed calculation of the nuclear density using the density distributions of S. Pieper and R. Wiringa [13].

3.2.1 Density using Uniform Sphere

The spatial extent of a nucleus is often approximated to a uniform sphere. Therefore, if all the nucleons were distributed evenly throughout the nucleus, the density would be uniform. The exact uniform sphere density values are available in Table 1 in Appendix A and the process for calculating these densities is also outlined in Appendix A.

When performing the nuclear matter extrapolation with respect to the density, either uniform sphere or calculated, it is necessary to compare to $\rho * (A-1)/A$ where ρ is the density and A is the atomic mass number. The reason this is necessary is because, if only ρ is considered, then we are not taking into account the fact that we have struck one nucleon. This struck nucleon must be removed from the density when comparing to a cross section. The (A-1)/A ratio is a scaling factor.

In order to minimize the error incurred during the linear fitting process the horizontal axis is $0.17 - \rho * (A-1)/A$. Therefore, the nuclear matter extrapolation can be the vertical axis intercept. If only $\rho * (A-1)/A$ is used, in order to extrapolate to 0.17, the error on the extrapolation involves both the uncertainty from the fit of the slope and the vertical intercept. The error in this extrapolation is significantly higher than if the horizontal variable is $0.17 - \rho * (A-1)/A$ and so the latter is used to minimize the error due to the fit. This is also used for the nuclear matter extrapolation with respect to the calculated densities. An example of this extrapolation is demonstrated in Figure 9.

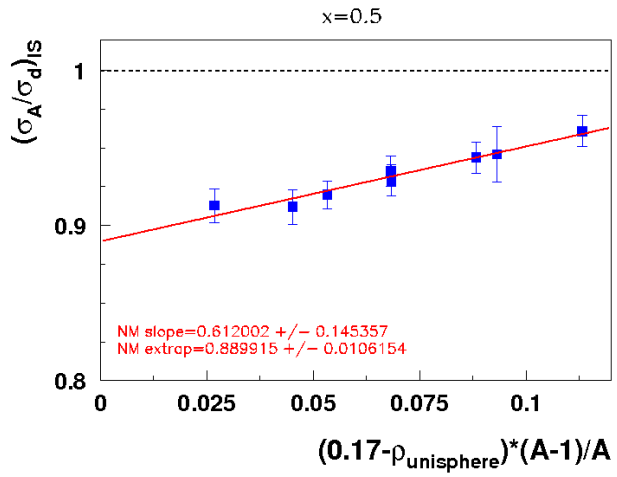

Figure 9: The EMC ratio for nuclear matter extrapolated to the y intercept from SLAC E139 with $Q^2 = 5$ and x = 0.5, when the EMC ratio is plotted against uniform sphere density.

3.2.2 Density using Calculated Densities

The most detailed calculation of nuclear densities was performed by S. Pieper and R. Wiringa [13] for the lighter nuclei and S. Pieper performed those for heavier nuclei. The light nuclei densities are calculated exactly while the heavy nuclei densities are extracted

from experimental data. The details of this calculation are described in Appendix A. The calculated densities will be used for all subsequent nuclear matter extrapolations since these are the most accurate density distributions available. An example of the extrapolation using the calculated density is demonstrated in Figure 10.

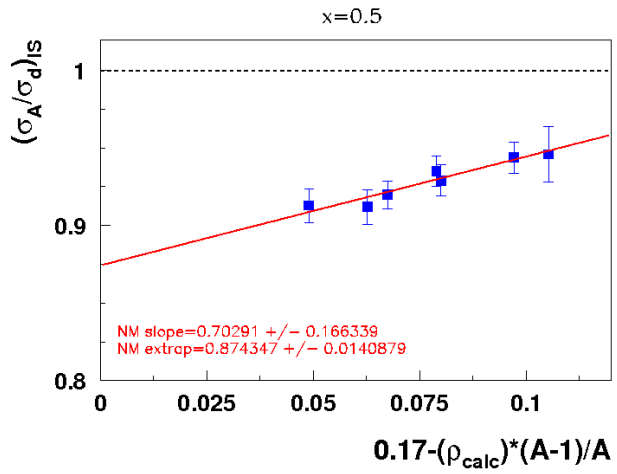

Figure 10: The EMC ratio for nuclear matter extrapolated to the y intercept from SLAC E139 with $Q^2 = 5$ and x = 0.5, when the EMC ratio is plotted against the more evolved density calculation.

3.3 Nuclear Matter Extrapolation with Coulomb Corrections

Another reason, other than theoretical comparison, that the extrapolation to nuclear matter is important in this case is that nuclear matter will be most affected by Coulomb corrections. Since Coulomb corrections increase with the atomic mass of the material, it will be highest for nuclear matter with infinite nuclear mass and constant nuclear density. In order to apply Coulomb corrections to the nuclear matter extrapolation, it is necessary to apply the Coulomb corrections to each nuclei individually. The extrapolation is then performed a second time using the new Coulomb corrected data. For example, Figure 11(a) and 11(b) illustrates the difference in the Coulomb corrected nuclear matter extrapolation(right) from the original non-corrected extrapolation(left).

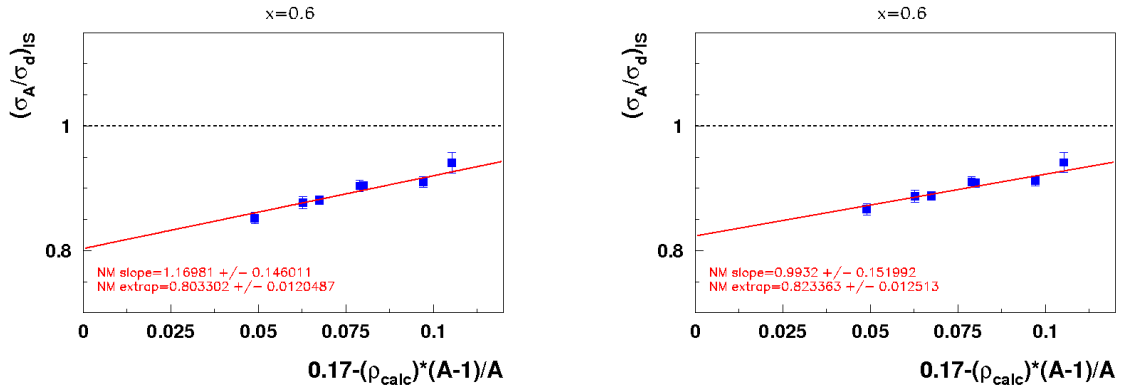

(a) (b)

Figure 11: Nuclear matter Extrapolation of the EMC effect. (a) illustrates the non-corrected extrapolation while (b) illustrates the corrected extrapolation. These plots correspond to SLAC E139 with $Q^2 = 5$ and x = 0.6.

4 Error Analysis Strategies

Radiative corrections had previously been made by the authors of [4] for the SLAC experiment and the data available for the JLab experiment also had all radiative corrections applied. These corrections are due to interactions within the nucleus that are not the one photon exchange between the incident electron and the nucleon. This may include a number of interactions including Bremstrahlung, two photon exchange, multiple photon emission, or exchange of soft photons as the electron enters or exits the nucleus. Thus, when these corrections were applied, the resulting data was that which only accounted for the single photon exchange with the struck quark. In addition to these corrections, there are also a number of other factors that contribute to uncertainties in measurements.

4.1 Statistical Uncertainty

Each data point includes various causes for uncertainty. Firstly, there will be a statistical uncertainty associated with each data point for the ratios of cross sections. Each point is subject to random changes in a measurement, which is dependent upon the number of data points taken.

4.2 Point to Point Uncertainty

Each point is also subject to a systematic uncertainty based on the equipment where the data was collected. For the SLAC E139 experiment, the first systematic uncertainty taken into account is a point to point uncertainty. Point to point uncertainties are those which are caused by the vertical position of the nuclei in the targets. These include fluctuations in beam energy, angle, and current, the scattered energy, spectrometer angle, acceptance of the detector, detector efficiency, background electron/positron pairs, neutron excess, and the radiative corrections. Each of these systematic errors were combined to a total point to point systematic error for each nuclei and added in quadrature to the statistical uncertainties by the authors of [4].

4.3 Target to Target Uncertainty

The second systematic uncertainty is the target to target systematic errors. Since this analysis is of a ratio of two targets, each having different densities and dimensions, uncertainties must be taken into consideration. The target is in three dimensions and so when comparing the targets, there is a normalization that must be accounted for. Each target had a separate normalization error. Thus, when extrapolating to nuclear matter, it was necessary to obtain the extremum of errors associated with the extrapolation. The method used was to add the normative error to the first half of the cross section ratios and subtracting the normative errors from the second half of the cross section ratios. This would obtain either the upper limit or the lower limit of the extrapolated ratio caused by the target to target uncertainties. The opposite was done for the other limit. This was performed at each x value. An example is illustrated in Figure 12. The error gathered from this target to target error analysis was added in quadrature to the first systematic error and the statistical error.

All data from JLabE03 103 included systematic and statistical error. These errors were added in quadrature to combine to a total error for each data point. This process was used to calculate all errors which were used in the extrapolations to nuclear matter.

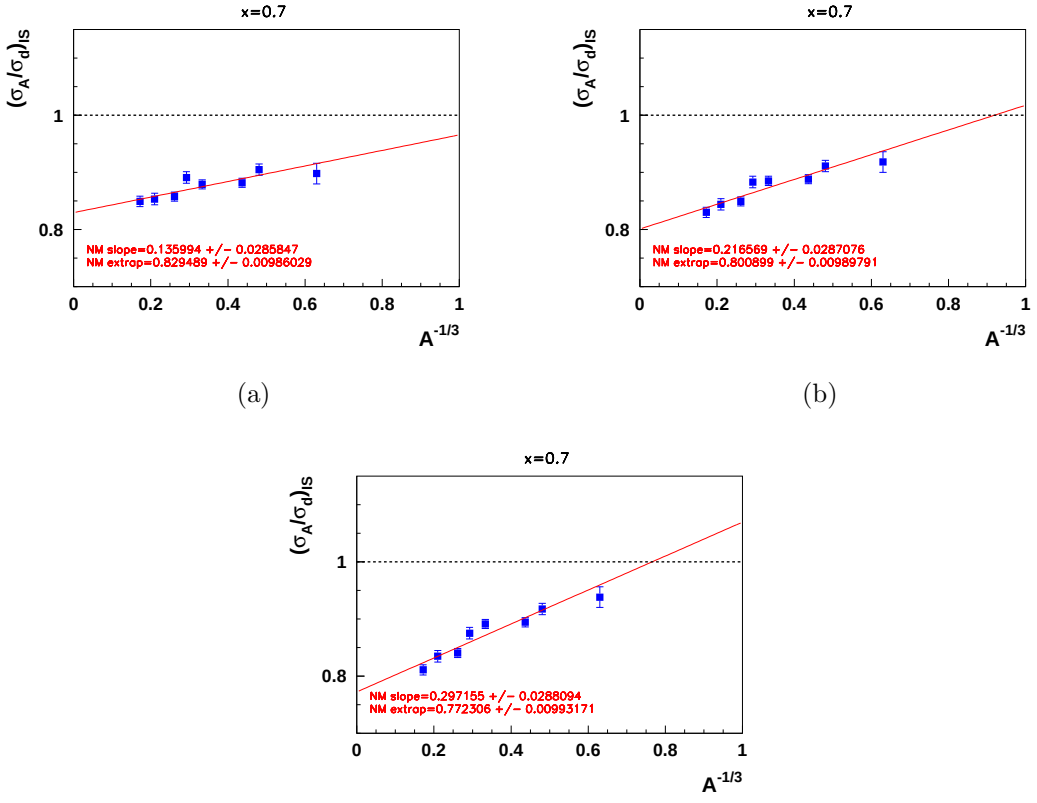

Figure 12: (a), (b), and (b) show the three steps to finding the normative error. (a) is an example of the smallest slope and the largest ratio possible with these errors. (b) is the original ratio extrapolation. (c) is an example of the largest slope and the smallest ratio possible with these errors. The difference between the extrapolated ratios in (c) and (b) as well as between those in (a) and (b) are the total normative errors added in quadrature

5 Kinematic Dependence

The two experiments, SLAC E139 and JLab E03 103, were performed at very different kinematics. Therefore, it is not possible to compare the two experiments directly. The energies and angles used were quite different. However, the value of Q^2 for the two experiments were similar and some of the x values taken into consideration were the same.

Q^2 for the SLAC experiment was 5 GeV/c^2 while Q^2 for the JLab experiment varied from 3.4 to 5.1 GeV/c^2 for the x region analyzed. Since these Q^2 values are quite similar in value, the structure function dependence on Q^2 is quite small. Therefore, we do not consider Q^2 to be a limiting factor in comparing these two experiments and since the difference is negligible it is not required to perform Q^2 evolution on either experiment.

5.1 Epsilon

Though Q^2 is not an important kinematic factor to analyze dependence on ϵ may be. Epsilon, as first introduced in Equation 5, is an important kinematic factor. It changes significantly between the two experiments and even within each experiment. Though ϵ is dependent upon Q^2 and ν, the most important dependency of epsilon is on θ, the scattering angle. Physically, the value of ϵ is the ratio of the longitudinal to transverse polarization of the virtual photon exchanged. ϵ can be related to the cross section through a rewriting of the cross section equation. This is described in a bit more detail in Appendix B. However, we may consider ϵ as an important kinematic value sensitive to each experiment. If the two experiments are considered, it must be established that either there is no epsilon dependence of the EMC ratio or, if there is epsilon dependence, a method for removing this dependence is necessary.

5.2 Coulomb Correction Dependence on Epsilon

Firstly, we look at the dependency of the Coulomb correction to the ϵ. To do this, we simply compare, for fixed nuclei and x, the Coulomb correction factor to ϵ. An x value of 0.5 is used since, at this kinematic x, two epsilon measurements are available for the SLAC data for three nuclei and two epsilon measurements for the JLab data. Figure 13 illustrates the Coulomb correction for a gold nuclei target at x=0.5 and $Q^2 = 5GeV^2$. There is a clear correlation between the Coulomb correction factor and the value of ϵ. This suggests that if Coulomb corrections are applied to all data, it may be possible to apply these Coulomb corrections to decrease the epsilon dependence of the EMC ratio, if it exists.

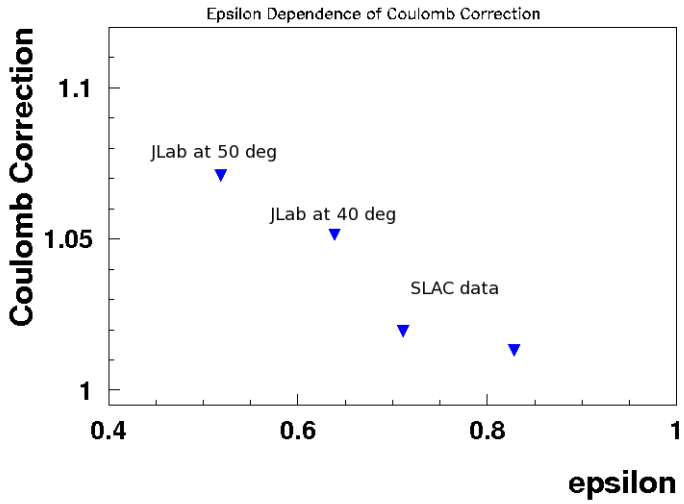

Figure 13: Example of Coulomb correction factor dependence on epsilon (gold nuclei at x=0.5 and $Q^2 = 5$. The trend for all other nuclei is similar.

5.3 EMC Ratio Dependence on Epsilon

In order to determine whether or not this epsilon dependence is also present in the EMC ratio, it is necessary to perform the nuclear matter extrapolation at each epsilon. Since nuclear matter extrapolation is only applicable at fixed x and Q^2, it is necessary to look for fixed x where there is EMC ratio data available for the most epsilon values. Due to the limitations in the SLAC data, the only x value with more than three targets is x=0.5. There were only four epsilon values, two from the SLAC data set and two from the JLab data set, however, this was sufficient for this analysis. There are only three nuclear targets where data is available for all four epsilon values. Therefore, these are the only targets used in the extrapolation.

Since the two experiments had a slightly different set of targets, it was necessary to take similar targets for that target which was different. Since copper and iron have a similar number of protons and mass number, they are considered to be similar nuclei. Therefore, iron, helium-4, and gold are used for the epsilons from the SLAC data set and copper, helium-4, and gold are used for the epsilon values from the JLab data set.

Figure 14 illustrates an example of the extrapolation. This was performed for each epsilon to generate Figure 15.

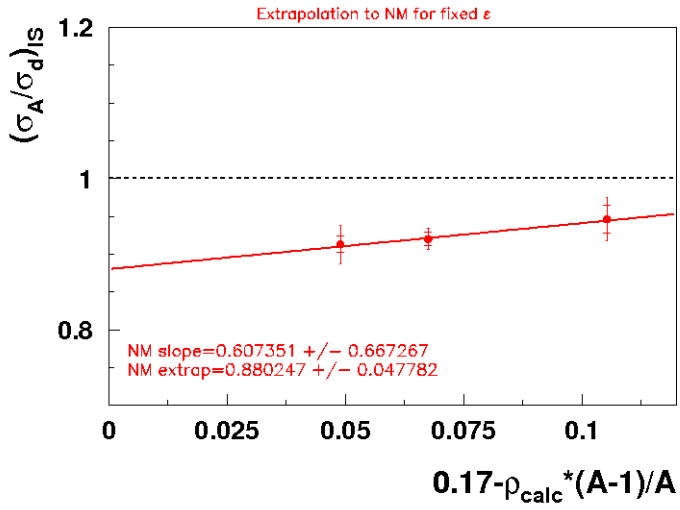

Figure 14: The EMC ratio can be extrapolated to nuclear matter for fixed epsilon. This plot is an example of such an extrapolation for $\epsilon = 0.828$, x = 0.5, and $Q^2 = 5$. This epsilon value is from SLAC E139.

Figure 15 shows a clear epsilon dependence of the EMC Ratio for nuclear matter. This shows that the EMC ratio is influenced greatly by the value of epsilon since, for the same x and Q^2, the EMC ratio has a span of approximately 0.10 over the range of measured epsilon.

Since the Coulomb correction factor was shown to be dependent upon this epsilon value as well, we apply the Coulomb corrections to each EMC ratio for each target at each epsilon and re-analyze the data as in extrapolations like Figure 14. When we apply the Coulomb corrections to each EMC ratio, the dependence of the nuclear matter EMC ratio on epsilon is removed from the data. This is graphically illustrated in Figure 16.

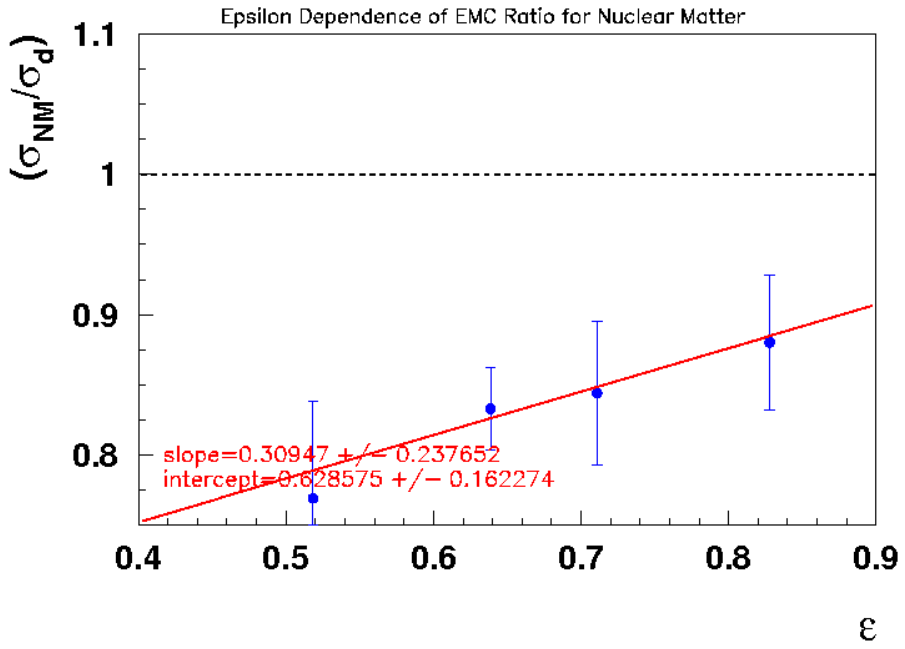

Figure 15: The extrapolation to nuclear matter performed for each of the epsilon values.

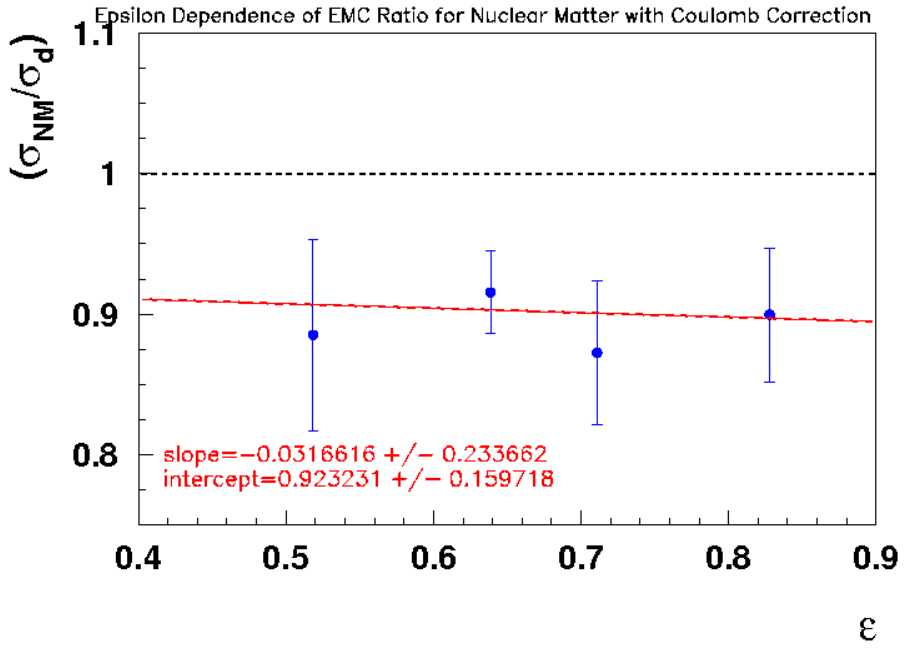

Figure 16: EMC ratio dependence on epsilon with Coulomb corrections are applied to the data.

6 Combining World Data

The previous section discussed how an application of the Coulomb corrections to the EMC ratios of each data set could greatly reduce, if not eliminate, the dependence of the EMC ratio on the kinematic factor epsilon. This suggests that it would be possible to use both experiments in the same extrapolation if Coulomb corrections are applied. When these Coulomb corrections are applied, there is little to no dependence on epsilon.

Now, the same nuclear matter extrapolation is performed with both data sets combined, as in Figure 17. This nuclear matter extrapolation was performed after the Coulomb correction had been applied individually to each data point. Thus, each experiment has been corrected for the differences in results caused by the individual experimental kinematics. Combining multiple experimental data sets is an important addition to the EMC effect analysis because it uses as much data as possible and so will give the most accurate experimental results.

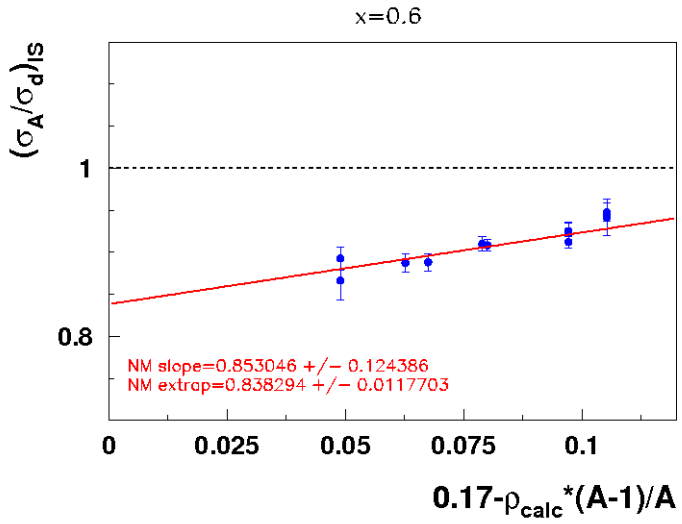

Figure 17: The EMC ratio for nuclear matter extrapolated to the y intercept of this plot from SLAC E139 and JLABE03 103 with $Q^2 = 5$ and x = 0.6.

This process is performed for every value of x between 0.4 and 0.7 that we have data for both the SLAC and JLab experiments (this is x = 0.4, 0.5, 0.6, and 0.7). These extrapolations are used to produce the EMC curve for nuclear matter as shown in Figure 18. Figure 18 also includes the theoretical calculations for the EMC effect as performed by Cloet [14]. Since the world data is now able to be combined, it is more accurate. Therefore, a comparison to theoretical calculations is possible.

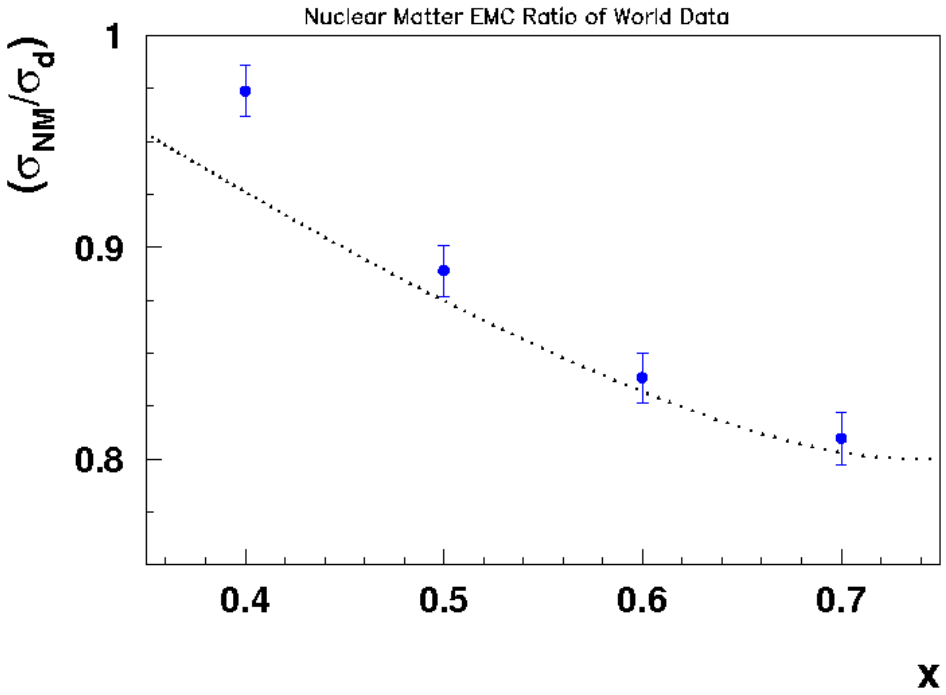

Figure 18: Nuclear matter extrapolation performed for each x with combined JLab and SLAC data,using Wiringa-Pieper density calculation. The dotted curve is the theoretical EMC calculation from Cloet [14].

7 Conclusion

When the European Muon Collaboration compared the scattering cross sections, in the deep inelastic scattering region,from iron to deuterium, they did not expect the ratio to deviate far from one. However, this was not the case and suggested new physics to be investigated. The EMC effect was born and theorists began to develop ideas to explain the surprisingly large effect. The effect suggests that the substructure of nucleons contained within a heavy nucleus is significantly different from free nucleons. This effect is still not, completely explainable by theory. Therefore, it is important that experimental data are as accurate as possible. It is also important to have a procedure for combining data from multiple experiments so that contributions from several sources are used to produce the experimental results.

This thesis project has successfully developed a methodology for applying Coulomb corrections in order to increase the accuracy of the EMC effect experimental data. These corrections are necessary especially for heavy nuclei and for experiments using low beam energies to access the DIS region.

Due to differing kinematics of experiments, it was previously incorrect to directly compare separate experiments. It became clear when comparing the EMC ratio with the kinematic variable ϵ. However, when the Coulomb corrections are applied, the dependence is removed. Therefore, data from different experiments can now be combined. Once the data has been combined, an extrapolation to nuclear matter allows for a comparison to

theoretical calculations. With this new methodology available, it is possible to combine world data for a more thorough analysis and comparison to theory.

Acknowledgments

The data for this report was gathered at SLAC National Accelerator Laboratory and Thomas Jefferson National Accelerator Facility. I would like to thank the Nuclear and Particle Physics Group at University of New Hampshire for supporting me for the last three years in my research endeavors. I especially thank Dr. Maurik Holtrop for introducing me to nuclear physics and always encouraging me to challenge myself and to have confidence. I would also like to express my appreciation for Dr. Karsten Pohl for the feedback he provided on the drafts of this thesis report. Lastly, I thank Dr. Patricia Solvignon for all the guidance she has given me from the time I started working with her. On this project, in particular, she motivated me to explore on my own while also encouraging me to ask any question I needed answered. She was quite patient and understanding of any difficulty I had.

References

[1] J.J. Aubert et al. The ratio of the nucleon structure functions $F2_n$ for iron and deuterium. *Phys.Lett.*, B123:275, 1983.

[2] I. Sick and D. Day. The EMC effect of nuclear matter. *Phys.Lett.*, B274:16–20, 1992.

[3] Patricia Solvignon. *Measurement of the 3He Spin Structure Functions in the Resonance Region: A Test of Quark-Hadron Duality on the Neutron.* PhD thesis, Temple University, 2006.

[4] J. Gomez, R.G. Arnold, Peter E. Bosted, C.C. Chang, A.T. Katramatou, et al. Measurement of the A-dependence of deep inelastic electron scattering. *Phys.Rev.*, D49:4348–4372, 1994.

[5] Jason Seely. *Precise Measurement of the Nuclear dependence of Structure Functions in Light Nuclei.* PhD thesis, Massachusetts Institute of Technology, 2006.

[6] Patricia Solvignon, Dave Gaskell, and John Arrington. Coulomb Distortion in the Inelastic Regime. *AIP Conf.Proc.*, 1160:155–159, 2009.

[7] John Arrington and Ingo Sick. Coulomb distortion in high-Q**2 elastic e-p scattering. *Phys.Rev.*, C70:028203, 2004.

[8] Andreas Aste, Cyrill von Arx, and Dirk Trautmann. Coulomb distortion of relativistic electrons in the nuclear electrostatic field. *Eur.Phys.J.*, A26:167–178, 2005.

[9] P.E. Bosted and V. Mamyan. Empirical Fit to electron-nucleus scattering. 2012.

[10] Andreas W. Aste. Coulomb distortion effects in quasi-elastic (e,e') scattering on heavy nuclei. *Nucl.Phys.*, A806:191–215, 2008.

[11] A. Daniel. EMC effect for light nuclei: New results from Jefferson Lab. *AIP Conf.Proc.*, 1374:455–458, 2011.

[12] O. Benhar, V.R. Pandharipande, and I. Sick. Density dependence of the EMC effect. *Phys.Lett.*, B469:19–24, 1999.

[13] Steven C. Pieper and R. B. Wiringa. Quantum monte carlo calculations of light nuclei1. *Annual Review of Nuclear and Particle Science*, 51(1):53–90, 2001.

[14] I.C. Cloet, Wolfgang Bentz, and Anthony William Thomas. Spin-dependent structure functions in nuclear matter and the polarized EMC effect. *Phys.Rev.Lett.*, 95:052302, 2005.

[15] R.G. Arnold, Peter E. Bosted, C.C. Chang, J. Gomez, A.T. Katramatou, et al. Measurements of the a-Dependence of Deep Inelastic electron Scattering from Nuclei. *Phys.Rev.Lett.*, 52:727, 1984.

[16] Donald F. Geesaman, K. Saito, and Anthony William Thomas. The nuclear EMC effect. *Ann.Rev.Nucl.Part.Sci.*, 45:337–390, 1995.

[17] C.W. De Jager, H. De Vries, and C. De Vries. Nuclear charge- and magnetization-density-distribution parameters from elastic electron scattering. *Atomic Data and Nuclear Data Tables*, 14(5–6):479 – 508, 1974. Nuclear Charge and Moment Distributions.

[18] G. Fey, H. Frank, W. Schütz, and H. Theissen. Nuclear rms charge radii from relative electron scattering measurements at low energies. *Zeitschrift für Physik*, 265(4):401–403, 1973.

Appendix A - Density of Each Target

The calculated densities are considered those which display the most accurate average densities for each nuclear target. For the heavier nuclei, $A \geq 12$, the following process was used to calculate the average density as shown in the third column of Table 1.

The average density of neutrons (n) and protons (p) is:

$$\langle \rho_{n,p} \rangle = \frac{\int \rho_{n,p}^2 d^3r}{\int \rho_{n,p} d^3r} \tag{11}$$

The sum of the average neutron and proton densities is equal to the average nuclear density:

$$\langle \rho_n \rangle + \langle \rho_p \rangle = \langle \rho_A \rangle \tag{12}$$

However, it is necessary to correct for the finite size of the proton. The following calculation is sufficient to make such a correction:

$$\langle \rho_{A_eff} \rangle = \langle \rho_A \rangle * \left(\frac{\langle r \rangle}{r_{eff}} \right)^3, \tag{13}$$

where $r_{eff} = \sqrt{\langle r \rangle^2 + 0.9^2}$.

The uniform sphere density calculations were made using the assumption that the nucleons are distributed evenly through a sphere of average radius. Therefore, the density for each nucleus is calculated as follows and described in [4]:

$$\rho = \frac{3A}{4\pi Re^3}, \tag{14}$$

where

$$Re = \sqrt{\frac{5\langle r^2 \rangle}{3}}. \tag{15}$$

$\langle r^2 \rangle$ is the root mean square (rms) radius of the nucleus. The value for these rms radii were taken from various sources, mainly [18].These calculations were used to complete the second column of Table 1.

A	ρ (nucleons/fm^3) (Uniform Sphere)	ρ (nucleons/fm^3) (S. Pieper and R. Wiringa)
3.00	0.05033	0.06181
4.00	0.10248	0.08635
9.00	0.06391	0.05215
12.00	0.08922	0.07951
27.00	0.10559	0.09348
40.00	0.10441	0.09342
56.00	0.11877	0.10436
63.00	0.11967	0.11053
108.00	0.12596	0.10831
197.00	0.14395	0.12164

Table 1: Uniform sphere densities and calculated densities for selected targets.

Appendix B - Cross Section Dependence on Epsilon

$$\sigma \equiv \frac{d^2\sigma}{d\Omega dE'} = \frac{\alpha^2 cos^2\frac{\theta}{2}}{4E^2 sin^4\frac{\theta}{2}}\left(\frac{2}{M}F_1(x,Q^2)tan^2\frac{\theta}{2} + \frac{1}{\nu}F_2(x,Q^2)\right) \tag{16}$$

$$\sigma \equiv \frac{d^2\sigma}{d\Omega dE'} = \frac{\alpha}{2\pi^2 Q^2}\frac{E}{E'}\frac{\nu(1-x)}{1-\epsilon}\left(\sigma_T(x,Q^2) + \epsilon\sigma_L(x,Q^2)\right) \tag{17}$$

σ_L and σ_T are longitudinal and transverse virtual photo-absorption cross sections:

$$F_1(x,Q^2) = \frac{\nu(1-x)}{4\pi^2\alpha}M\sigma_T(x,Q^2) \tag{18}$$

$$F_2(x,Q^2) = \frac{\nu(1-x)}{4\pi^2\alpha}\frac{\nu}{1+\frac{\nu^2}{Q^2}}\left(\sigma_L(x,Q^2) + \sigma_T(x,Q^2)\right). \tag{19}$$

Appendix C - Extra Plots

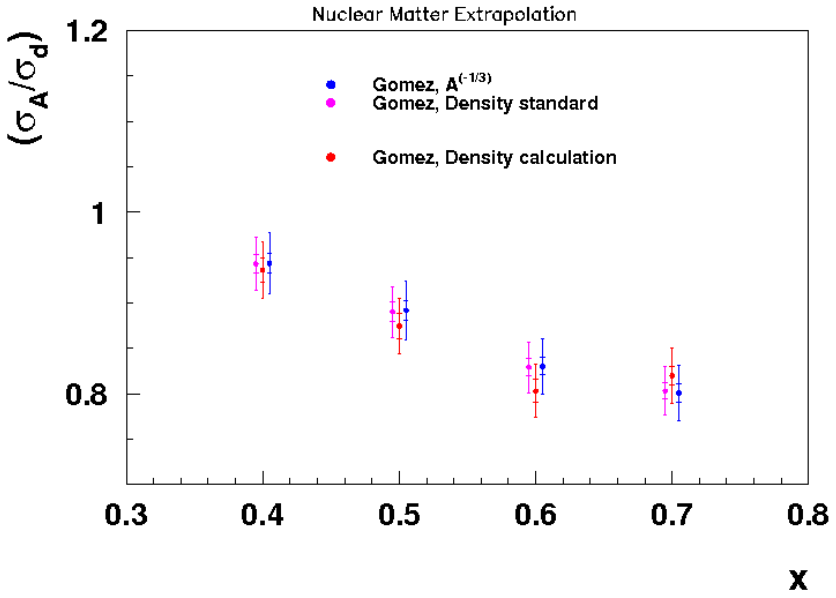

Figure 19: Extrapolation to nuclear matter performed by comparing the EMC ratios against $A^{-1/3}$ or through density calculations. This plot represents the EMC curve for the SLAC E139 data using the three extrapolation methods. Data points are adjusted for visiblity.

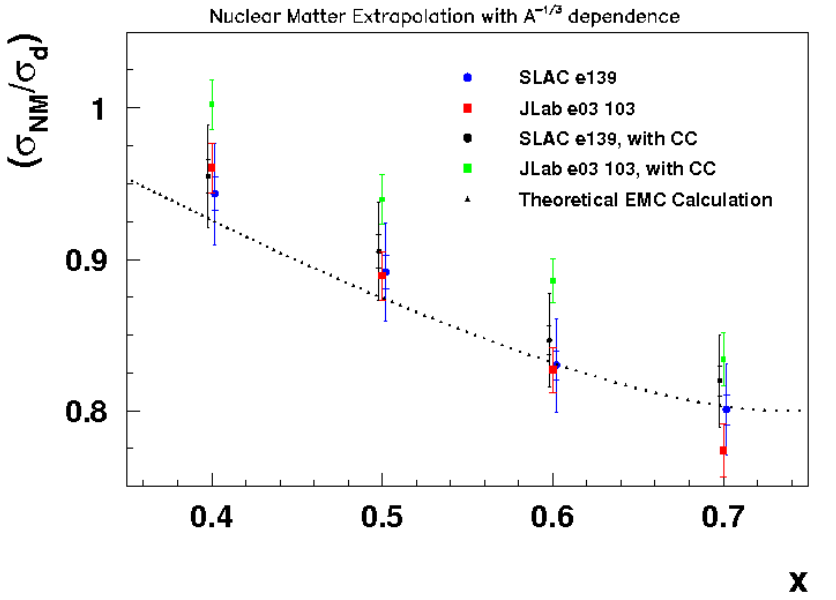

Figure 20: The EMC ratios calculated for each experiment seperately. The Coulomb corrections, when applied to the JLab experiment are far more significant than those for the SLAC experiment since the beam energy was smaller for the former. Data points are adjusted for visiblity.